Reduction of Radar Image Artifacts Caused by Target Inlets

Brett Borden

***Abstract*— The standard radar weak-scatterer model is inappropriate to targets with inlets and cavities and range-resolved images created using this model often display artifacts associated with these structures. Since inlets and cavities (typically) make a strong contribution to the radar field scattered from aircraft targets, these artifacts can confound the image interpretation process. Many of the more complete and accurate scattering models require extensive knowledge about the cavity/inlet shape and size and, moreover, are numerically intensive—features that make them unsuitable for many imaging applications. We examine an older (first-order) model based on a weak-scattering modal expansion of the structure which appears to be well suited to radar imaging.**

***Index Terms*—Inlets, radar cross section, radar imaging.**

I. Introduction

RADAR imaging systems often exploit the mathematical properties of a linear nondispersive model to recover an object function $\rho(x)$ from measured data $E(k)$ and even though modern *direct* scattering methods for cross-section prediction rarely use such a simple description, the problem of radar imaging is often well approximated by the so-called "weak point-scatterer" (linearized) model [1]. Moreover, the analytical convenience of this traditional approach is so compelling that it is often applied to radar situations for which it is known to be invalid (cf., [2], [3]).

Scattering bodies consisting of ducts or cavities can significantly deviate from the weak point-scatterer assumption. Typically, these re-entrant body elements are dispersive in the sense that the field scattered from these structures may contain frequency components whose velocity differs from the returns due to nondispersive target structures. Reconstructing such a $\rho(x)$ under the nondispersive assumption results in unwanted image artifacts (displaced in time/position with respect to their "expected" location), which are sometimes difficult to associate with specific target features and which may obscure other (correctly modeled) image elements. Owing to the importance of ducts and cavities in airborne target image reconstruction (they often contribute the strongest part of the radar return) a significant effort has been made to accurately model and predict their scattering behavior (cf., [4]–[7]). Such direct scattering approaches are often inappropriate, however, because their complexity makes them computationally unwieldy when applied to image reconstruction of unknown targets.

Below, we examine an old and relatively simple model for duct and cavity scattering. We will demonstrate how this model leads to a very easy interpretation of the first-order properties of radar scattering from cavities and inlets while maintaining much of the complexity seen in actual radar data. Using this model, we develop a simple method for filtering-out the dispersive effects due to inlets and cavities. Our approach is related to recent dispersive-scatterer identification methods [8]–[10] but is easily extended to target parameter identification and (may) prove useful in target recognition problems.

Manuscript received July 2, 1997; revised January 19, 1999. This work was supported by the Office of Naval Research.

The author is with the Research and Technology Group, Naval Air Warfare Center Weapons Division, China Lake, CA 93555 USA.

Publisher Item Identifier S 0018-926X(99)04840-1.

II. Radar Scattering

In a monostatic scattering situation it can be shown [1] that the weak scatterer far-field response $E(k)$ due to an harmonic excitation of a target can be written

$$E_{\text{scatt}}(k) \approx \int_{\mathbb{R}^2} \rho(x') e^{i2kx'}\, dx'. \tag{1}$$

This is a linear superposition of waves radiating from locations in the target with scatterer strength proportional to $\rho(x)$. The incident wave has: angular frequency ω; speed c; wave number $k = \omega/c$; and the factor of two accounts for the two-way travel distance from the radar to the target and back again.

When a high level of system resolution and sensitivity is required, the limitations of the (analytically "convenient") model of (1) can adversely affect the target recognition process by mapping interacting (nonweak) and/or dispersive frequency-domain scattered field components to an "incorrect" target image location [3], [4]. Because of its ease of interpretation, however, it is sometimes advantageous to save as much of the "fixed point-scatterer" nature of ρ as we can. This has been traditionally accomplished by fixing an *effective* phase center to a single location on the target and attributing any anomolous variations in the image to a dispersive phase term in the radar signal. In this way, target position shifts are accounted for by a general dispersion relation. With this modification, (1) can be written

$$E_{\text{scatt}}(k) \approx \int_{\mathbb{R}^2} \rho(x') W(x', x''), e^{-i2kx'}\, dx'\, dx'' \tag{2}$$

where

$$W(x', x'') = \int_{k_1}^{k_2} S(x', k') e^{i(2k'x' - 2\beta(x', k'))} e^{i2k'(x'' - x')}\, dk' \tag{3}$$

$S(x',k') \leq 1$ accounts for varying strength and (k_1,k_2) represents the data (bandwidth) limits. Equations (2) and (3) show how the effects of complex scattering centers can be interpreted as being due to a spatially varying point-spread function $W(x,x')$ acting on an object function consisting of weak, isotropic, and frequency-*independent* scatterers fixed at effective phase-center locations on the target.

The propagation speed of electromagnetic waves in ducts, inlets, and cavities displays a general dependence on frequency. The geometry of these structures (modeled here as waveguides) defines so-called "cutoff frequencies" and the speed of waves in the waveguide varies from zero (when the frequency equals the cutoff frequency) to c (when the frequency is much larger than cutoff [11]). The point-spread function (3) associated with terminated waveguides of effective length L with entrance located at x_{inlet} (which we shall take as the phase center associated with this structure) can be expressed as a modal expansion [6]

$$S(x,k)e^{i(2kx-2\beta(x,k))} \rightarrow \frac{1}{k}\sum_{m=1}^{M} S_m(k)e^{i(2kx-2\beta_m(x,k))}. \tag{4}$$

The phase term β_m depends upon the cutoff frequencies $\omega_{c,m} = ck_{c,m}$, which are labeled by the mode indexes m. The cutoff frequencies also allow us to limit the terms in the modal sum to $M = \max\{m | k_{c,m} \leq k_2\}$. The weak-scatterer approximation yields

$$2\beta_m(x,k) = \begin{cases} 2kx + 2L\sqrt{k^2 - k_{c,m}^2}, & \text{if } x = x_{\text{inlet}} \\ 2kx, & \text{otherwise.} \end{cases} \tag{5}$$

If we assume that S_m is a slowly varying function of k (in comparison to the phase term), then applying this result yields [from (2)]

$$\hat{\rho}(x) \approx \int_{\mathbb{R}^2} dx'\ \rho(x') \cdot \begin{cases} \displaystyle\sum_{m=1}^{M} S_m \int_{k_1}^{k_2} k^{-1} e^{-i2L\sqrt{k^2-k_{c,m}^2}} e^{i2kx}\, dk \\ \quad \text{if } x' = x_{\text{inlet}}; \\ \operatorname{sinc}(\Delta k(x-x'))e^{i2\overline{k}(x-x')} \\ \quad \text{otherwise} \end{cases} \tag{6}$$

where $\overline{k} = (k_1 + k_2)/2$ and $\Delta k = k_2 - k_1$.

The image $\hat{\rho}(x)$ can be understood in terms of the object $\rho(x)$ by examining the integral

$$I_m(x) = \int_{k_1}^{k_2} k^{-1} e^{-i2L\sqrt{k^2-k_{c,m}^2}} e^{i2kx}\, dk. \tag{7}$$

If we substitute [12]

$$e^{-i2L\sqrt{k^2-k_{c,m}^2}} = 2i\sqrt{k^2 - k_{c,m}^2} \int_L^\infty \cdot J_0(2k_{c,m}\sqrt{x''^2 - L^2}) e^{-i2kx''}\, dx'' \tag{8}$$

where $J_0(\xi)$ is the Bessel function of the first kind, then we can write

$$I_m(x) = 2i \int_L^\infty dx''\ J_0(2k_{c,m}\sqrt{x''^2 - L^2}) \cdot \int_{\max(k_1,k_{c,m})}^{k_2} dk\ \sqrt{1-(k_{c,m}/k)^2}\, e^{i2k(x-x'')}. \tag{9}$$

If we further make the approximation (see [13] for details)

$$\int_{\max(k_1,k_{c,m})}^{k_2} \sqrt{1-(k_{c,m}/k)^2}\, e^{i2k(x-x'')}\, dk \approx \alpha\Delta k_{(1,c)}\ \operatorname{sinc}(\Delta k_{(1,c)}(x-x''))e^{i2\overline{k}_{(1,c)}(x-x'')} \tag{10}$$

where $\overline{k}_{(1,c)} = (\max(k_1, k_{c,m}) + k_2)/2$ and $\Delta k_{(1,c)} = k_2 - \max(k_1, k_{c,m})$, then it is easy to see that the down-range effects of the inlet will appear as the function $J_0(x)$, shifted according to $x \rightarrow \sqrt{x^2 - L^2}$, dilated by $x \rightarrow 2k_{c,m}x$, and "blurred" by the $\operatorname{sinc}(\Delta k_{(1,c)}x)$ function.

III. Parameter Extraction

The $\mathcal{Y}_\nu$ transform can be employed to show that [12]

$$\pi\kappa \int_L^\infty J_0(2k_{c,m}\sqrt{x^2-L^2})x^n Y_{-1}(2\kappa x)\, dx = \begin{cases} K_0(2L\sqrt{k_{c,m}^2 - \kappa^2}) & \text{if } k_{c,m} > \kappa \\ -\dfrac{\pi}{2}(-1)^n Y_0(2L\sqrt{\kappa^2 - k_{c,m}^2}) & \text{if } \kappa > k_{c,m} \end{cases} \tag{11}$$

where $Y_\nu(\xi)$ is the Bessel function of the second kind (of order ν), $K_0(\xi)$ is the modified Bessel function of order zero, and $n = 0, 1, \cdots, \infty$.

Since $K_0(\xi)$ and $-Y_0(\xi)$ both rise sharply to ∞ as $\xi \rightarrow 0$, this result suggests a method for extracting the parameters $k_{c,m}$ from the image $\hat{\rho}(x) \sim S_L(x)J_0(2k_{c,m}\sqrt{x^2 - L^2})$ where $S_L(x)$ denotes the unit step at $x = L$. Define the transformation

$$\mathcal{P}_n(\kappa) = \pi\kappa \int_0^\infty \hat{\rho}(x)x^n Y_{-1}(2\kappa x)\, dx \tag{12}$$

for $\kappa > 0$. Then it is easy to see from (5)–(9) that $\mathcal{P}_n(\kappa)$ will be sharply peaked when $\kappa = k_{c,m}, k_1 \leq \kappa \leq k_2$.

The *reciprocal* transform to (12) is not quite as well defined. It can be shown [14], however, that

$$(\mathcal{H}_\nu f)(x) = \int_0^\infty f(\kappa)\boldsymbol{H}_\nu(x\kappa)(x\kappa)^{1/2}\, d\kappa \tag{13}$$

where $\boldsymbol{H}_\nu(x)$ is the Struve function, obeys $\mathcal{H}_\nu\mathcal{Y}_\nu = \mathcal{Y}_\nu\mathcal{H}_\nu = \mathcal{I}$ for functions in $L^2(0,\infty)$ when $-1 < \nu < 0$.

This parameter "isolation" method, together with the reciprocal transform of (13), is the basis of a filtering method for mitigating cavity related image artifacts.

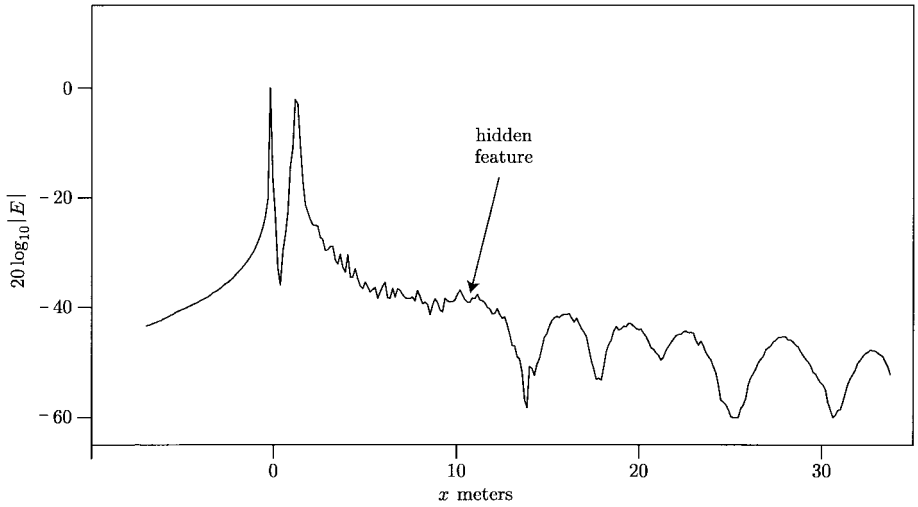

Fig. 1. Scattered field data (relative magnitude in decibels) from terminated waveguide.

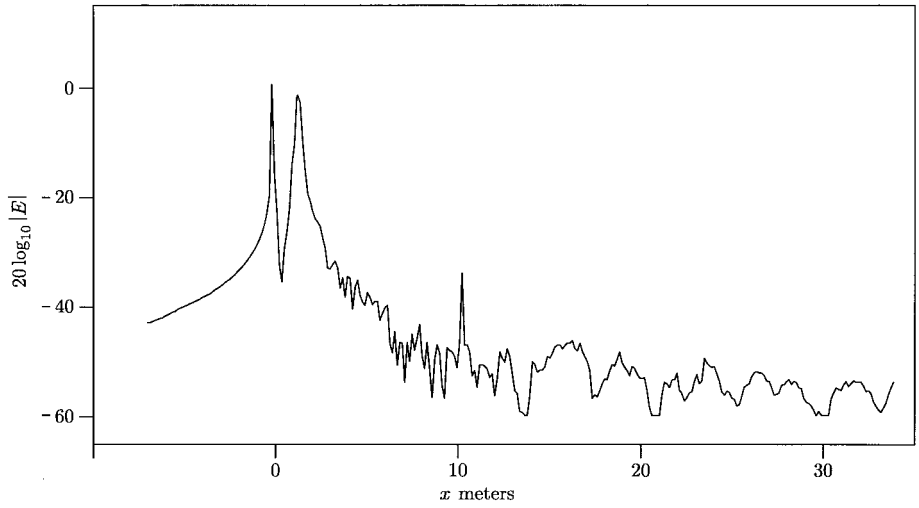

Fig. 2. "Cleaned" image corresponding to Fig. 1 (relative magnitude in decibels).

IV. Some Experimental Results

We launched a (stepped-frequency) pulse at the open end of a terminated 103-cm length of WR 284 rectangular waveguide. Fig. 1 shows the scattered return from the waveguide when the frequency band was 12.16–13.26 GHz. Plotted is the magnitude of the Fourier transform of the scattered field data. The duct-related artifacts can be seen extending for many multiples of the length of the target. For test purposes, we introduced an additional artificial signal into the measured data. This signal was generated (in the frequency domain) by simply adding the complex array generated by $0.02\exp(i2k_j * 10)$ and corresponds to a point scatterer located at range $x = 10$ m with strength less than that of the duct artifacts (so that it cannot be seen in Fig. 1).

The image artifacts in Fig. 1 are to be reduced by filtering in the $\mathcal{P}_n$-transform domain. As part of our initial investigation, we applied a simple truncation filter: $\{\mathcal{P}_n(\kappa)\colon |\mathcal{P}_n(\kappa)| > \tau\} \rightarrow 0$ where τ is a user defined threshold. Fig. 2 is the "cleaned" reconstruction formed by inverting the filtered results with $\tau = 0.3$. Note that the point scatterer at $x = 10$ m is now clearly visible and that the duct-related artifacts have indeed been reduced.

V. Discussion and Conclusion

In the context of radar imaging, the effective goal of many *direct* scattering efforts can be viewed as that of estimating the (effective) parameters L and $\{k_{c,m}\}$. These parameters encapsulate the cavity/inlet size- and shape-induced behavior of the radar scattered field. Of course, once these parameters are identified, the model of equation (6) is determined and the radar imaging artifacts in $\hat{\rho}(x)$ can be ameliorated.

In addition to this parametric description of scattering from re-entrant structures, we have begun a preliminary examination of robust methods for filtering the scattering artifacts without eliminating those target structures that might be buried beneath the artifacts. This artifact mitigation method is based on the $\mathcal{Y}_\nu$ and Struve transforms and has yet to be fully characterized. For illustration purposes, however, we applied a simple (threshold truncation) filter and have shown the artifacts associated with a truncated waveguide to be reduced by about 10 dB (compare

Figs. 1 and 2). The question of "optimal" reduction is still open, as is the issue of alternate filtering approaches.

REFERENCES

[1] B. Borden, "Some issues in inverse synthetic aperture radar image reconstruction," *Inverse Problems*, vol. 13, p. 571, 1997.

[2] G. Dural and D. L. Moffatt, "ISAR Imaging to identify basic scattering mechanisms," *IEEE Trans. Antennas Propagat.*, vol. 42, p. 99, Jan. 1994.

[3] A. W. Rihaczek and S. J. Hershkowitz, *Radar Resolution and Complex-Image Analysis*. Dedham, MA: Artech House, 1996.

[4] H. R. Witt and E. L. Price, "Scattering from hollow conducting cylinders," *Proc. Inst. Elec. Eng.*, vol. 115, p. 94, Jan. 1968.

[5] J. W. Moll and R. G. Seecamp, "Calculation of radar reflecting properties of jet engine intakes using a waveguide model," *IEEE Trans. Aerosp. Elect. Syst.*, vol. 6, p. 675, Sept. 1969.

[6] C.-C. Huang, "Simple formula for the RCS of a finite hollow circular cylinder," *Electron. Lett.*, vol. 19, p. 854, 1983.

[7] H. Ling, R.-C. Chou, and S. W. Lee, "Shooting and bouncing rays: Calculating the RCS of an arbitrary cavity," *IEEE Trans. Antennas Propagat.*, vol. 37, p. 194, Feb. 1989.

[8] A. Moghaddar and E. K. Walton, "Time-frequency distribution analysis of scattering from waveguides," *IEEE Trans. Antennas Propagat.*, vol. 41, p. 677, May 1993.

[9] L. Carin, L. B. Felsen, D. Kralj, S. U. Pillai, and W. C. Lee, "Dispersive modes in the time domain: Analysis and time-frequency representation," *IEEE Microwave Guided Wave Lett.*, vol. 4, p. 23, Jan. 1994.

[10] L. C. Trintinalia and H. Ling, "Joint time-frequency ISAR using adaptive processing," *IEEE Trans. Antennas Propagat.*, vol. 45, p. 221, Feb. 1997.

[11] J. A. Stratton, *Electromagnetic Theory*. New York: McGraw Hill, 1941.

[12] A. Erdélyi, W. Magnus, F. Oberhettinger, and F. G. Tricomi, *Tables of Integral Transforms Volume II*. New York: McGraw-Hill, 1954.

[13] B. Borden, "Reduction of ISAR image artifacts caused by re-entrant structures," *Proc. SPIE Radar Processing, Technol., Applicat. II*, San Diego, CA, July 31–Aug. 1, 1997, vol. 3161, pp. 9–19.

[14] P. G. Rooney, "On the $\mathcal{Y}_\nu$ and $\mathcal{H}_\nu$ transformations," *Can. J. Math.*, vol. 32, no. 5, p. 1021, 1980.

Brett Borden, photograph and biography not available at the time of publication.